

Electronic Supplementary Information for
“Inorganic Nanotubes with Permanent Wall Polarization as
Dual Photo-Reactors for Wastewater Treatment with Simultaneous
Fuel Production”

Sabyasachi Patra,^{a,d,*} Delphine Schaming,^b Pierre Picot,^a Marie-Claire Pignié,^a Jean-Blaise
Brubach,^c Lorette Sicard,^b Sophie Le Caër,^{a,*} Antoine Thill^{a,*}

^a*Université Paris-Saclay, CEA, CNRS, NIMBE, 91191, Gif-sur-Yvette, France*

^b*Université de Paris, ITODYS, CNRS, UMR 7086, 15 rue J.-A. de Baïf, F-75013 Paris, France*

^c*Ligne AILES, Société civile Synchrotron SOLEIL, 91192 Gif sur Yvette, France*

^d*Radiochemistry Division, Bhabha Atomic Research Centre, Trombay, Mumbai - 400085, India*

*Corresponding Authors: Email: sabyasachi.patra@cea.fr; spatra@barc.gov.in (S.P.)

sophie.le-caer@cea.fr (S.L.C.)

antoine.thill@cea.fr (A.T.)

Contents	Page No.
TEM analysis	S1
SAXS analysis	S2
Parameters used to simulate the SAXS profiles of Imo-CH ₃ (without and with DBAN)	S2
Fourier Transform Infrared Spectroscopy characterization of Imo-CH ₃ and DBAN loaded Imo-CH ₃ nanotubes	S2
FT-IR spectrum of DBAN in KBr pellet	S3
FT-IR spectra of Imo-CH ₃ and DBAN encapsulated Imo-CH ₃ thin films	S4
Assignment of the vibrational bands of Imo-CH ₃ and DBAN	S5
UV-Vis absorption and fluorescence spectroscopy	S6
UV-Vis absorption spectra of DBAN in hexane	S6
Relative peak intensity between two peaks in UV-Vis spectrum of DBAN in hexane (a) and DBAN encapsulated in Imo-CH ₃ aqueous solutions (b-d)	S6
Determination of loading concentration of DBAN in Imo-CH ₃ nanotubes	S7
Wavelength maxima in UV-Vis absorption spectra of DBAN	S8
Relative intensity between peaks measured in the fluorescence emission spectrum of DBAN in hexane (a) and DBAN encapsulated in Imo-CH ₃ in aqueous solution (b-d)	S9
Wavelength maxima in fluorescence emission spectra of DBAN	S10
Evolution of UV-Vis absorption spectra of DBAN in hexane, pre-bubbled with oxygen and argon, upon UV illumination	S11
Relative absorption at two different wavelength during UV illumination of air saturated solution of DBAN in hexane	S12
Evolution of UV-Vis absorbance at different wavelengths for encapsulated DBAN at varying loading concentrations	S13
Fitting of kinetic curves	
Time variation of inverse of DBAN concentration in Imo-CH ₃ solution under UV illumination	S14
Rate constants for photo-oxidation, photo-cycloaddition and photo-oxidation quantum yield	S15
Comparison of UV-Vis absorption spectra of DBAN in water and of encapsulated DBAN in Imo-CH ₃ aqueous solution	S16
Stability of Imo-CH ₃ nanoreactor under UV illumination	S17
Possible mechanism of DBAN mineralization	S19
References	S19

1. TEM analysis

Sample for conventional TEM was prepared by deposition of a 5 μL drop of aqueous Imo-CH₃ suspension ($\sim 80 \text{ mg}\cdot\text{L}^{-1}$) on a carbon film coated copper grid. After 10 seconds, the excess liquid was soaked up with a filter paper. Transmission electron microscopy (TEM) was carried out using a Philips CM12 electron microscope at an operating voltage of 80 kV. For Cryo-TEM, a 5 μL drops of the aqueous imo-CH₃ suspension was deposited on EM grids covered with a holey carbon film (Quantifoil R2/2) previously treated with a plasma glow discharge. The excess liquid on the grid was soaked up with filter paper, and subsequently the grid was quickly immersed in liquid ethane to form a thin vitreous ice film. The overall procedure was executed using a Vitrobot apparatus (FEI Company). The microscopic observations were made at low temperature (-180°C) on a JEOL 2010 FEG microscope operated at 200 kV. A Gatan camera was used to collect the images in both conventional and cryo-TEM.

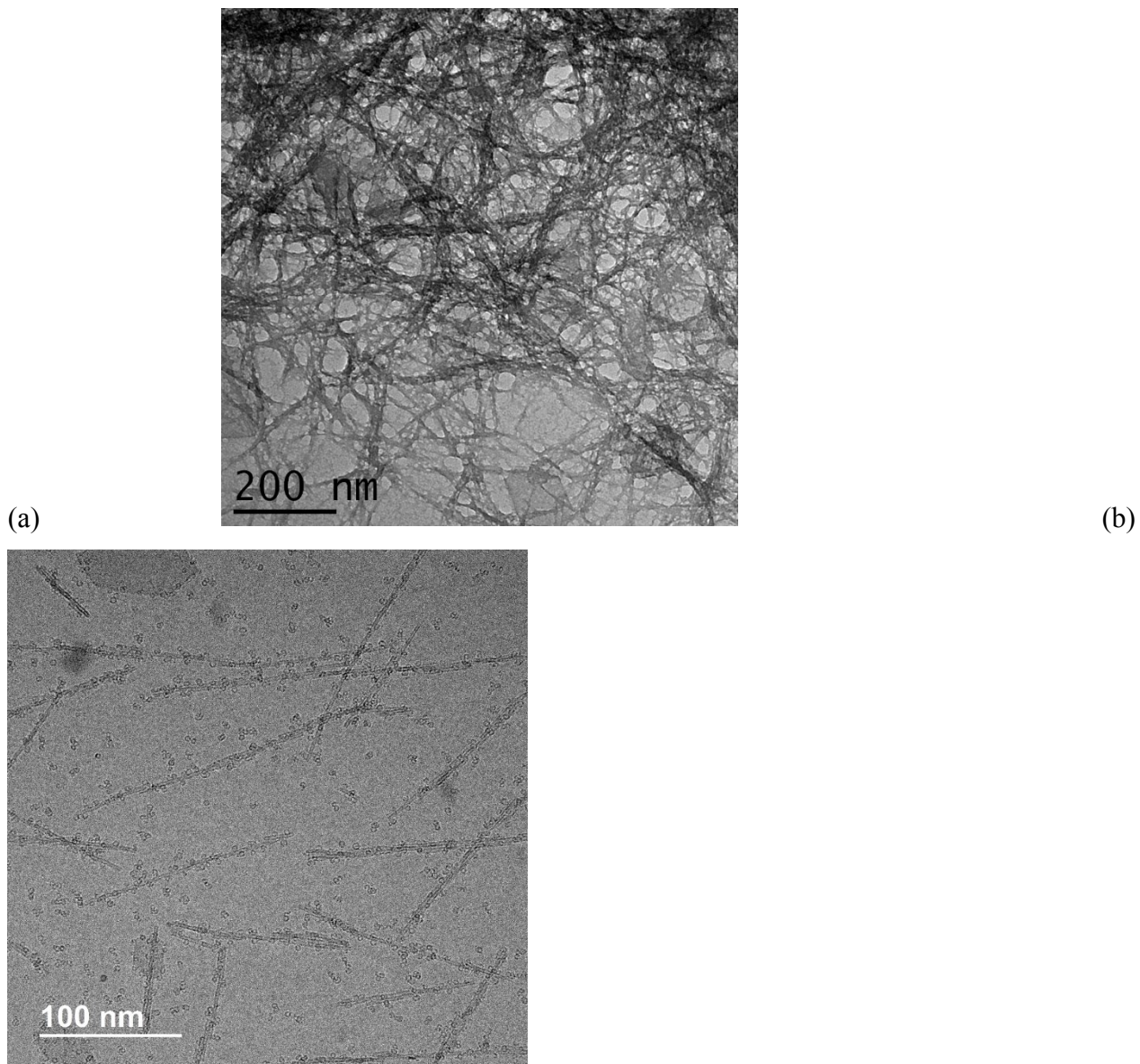


Figure S1. Conventional TEM image of dried suspensions (a) and Cryo-TEM image of the hydrated (b) Imo-CH₃ nanotubes. The small spherical objects in the Cryo-TEM image are proto-imogolites which are produced in small quantities along with the nanotubes.^{1,2}

2. SAXS analysis

Table S1. Parameters used to simulate the SAXS profiles of Imo-CH₃ (without and with DBAN).

Parameters	Values	
	Pristine Imo-CH ₃	DBAN@Imo-CH ₃
Internal radius (Å)	9.6	
Number of Si atom per ring (N)	16	
Wall thickness (Å)	5.5	
Lattice parameter (Å)	4.3	
Internal electronic density (e ⁻ Å ⁻³)	0.15	0.21
External electronic density (e ⁻ Å ⁻³)	0.334	

3. Fourier Transform Infrared Spectroscopy (FT-IR) characterization of Imo-CH₃ and DBAN-loaded Imo-CH₃ nanotubes.

The encapsulation of DBAN in Imo-CH₃ nanotubes was also studied by infrared spectroscopy using a Bruker IFS125 Fourier Transform Infrared (FT-IR) spectrometer under vacuum. The IR studies were carried out on ultrathin films of imogolite, prepared using the procedure described in reference.³ Infrared absorbance spectra were recorded in the mid-infrared (MIR) range, from 500 to 4000 cm⁻¹ with 0.5 cm⁻¹ resolution using a KBr beamsplitter and a HgCdTe detector. All spectra result from averaging 200 scans measured with a mobile mirror speed of 2 cm·s⁻¹. Figure S2 gives the FT-IR absorption spectrum of DBAN only. In this case only, the sample was not under vacuum. Figure S3 gives the FT-IR spectra of thin films of pristine Imo-CH₃ nanotubes (a) and of Imo-CH₃ nanotubes loaded with DBAN at varying loading concentrations (b-d). Table S2 summarizes the FT-IR bands of Imo-CH₃ nanotubes and DBAN. Although the IR absorption bands of DBAN in the region of aromatic C-H bending (700 – 900 cm⁻¹) are intense, there is a considerable overlap of these bands with the intense Si-O-Al stretching band of Imo-CH₃ at 956/900 cm⁻¹. This makes it difficult to resolve the DBAN bands from the Imo-CH₃ bands in Figure S3(b-d). However, the increase in relative intensity between the Si-O stretching band and the O-H stretching mode (with a reproducible intensity due to a prior pumping) with increased DBAN loading (b-d) corroborates the contribution of IR absorption due to aromatic C-H bending of DBAN in the region of the Si-O stretching of Imo-CH₃ nanotubes. The IR absorption band due to the aromatic C=C bending (1700-1500 cm⁻¹) is weak even in pristine DBAN and could not be resolved in Figure S3(b-d). The IR absorption bands due to the aromatic C-H stretching of DBAN (~ 3030 cm⁻¹) are detected in the sample with the highest DBAN loading only (Figure S3d). The corresponding spectral region is

highlighted yellow in the enlarged view of the Figure. It is noteworthy that, the IR intensity of different vibrational bands of DBAN seems to have significantly reduced in presence of Imo-CH₃ nanotubes. This reduction in IR intensity maybe attributed to the dielectric screening by polar Imo-CH₃ sidewall, analogous to carbon nanotube.⁴ This corroborates the encapsulation of DBAN molecules in Imo-CH₃ cavity.

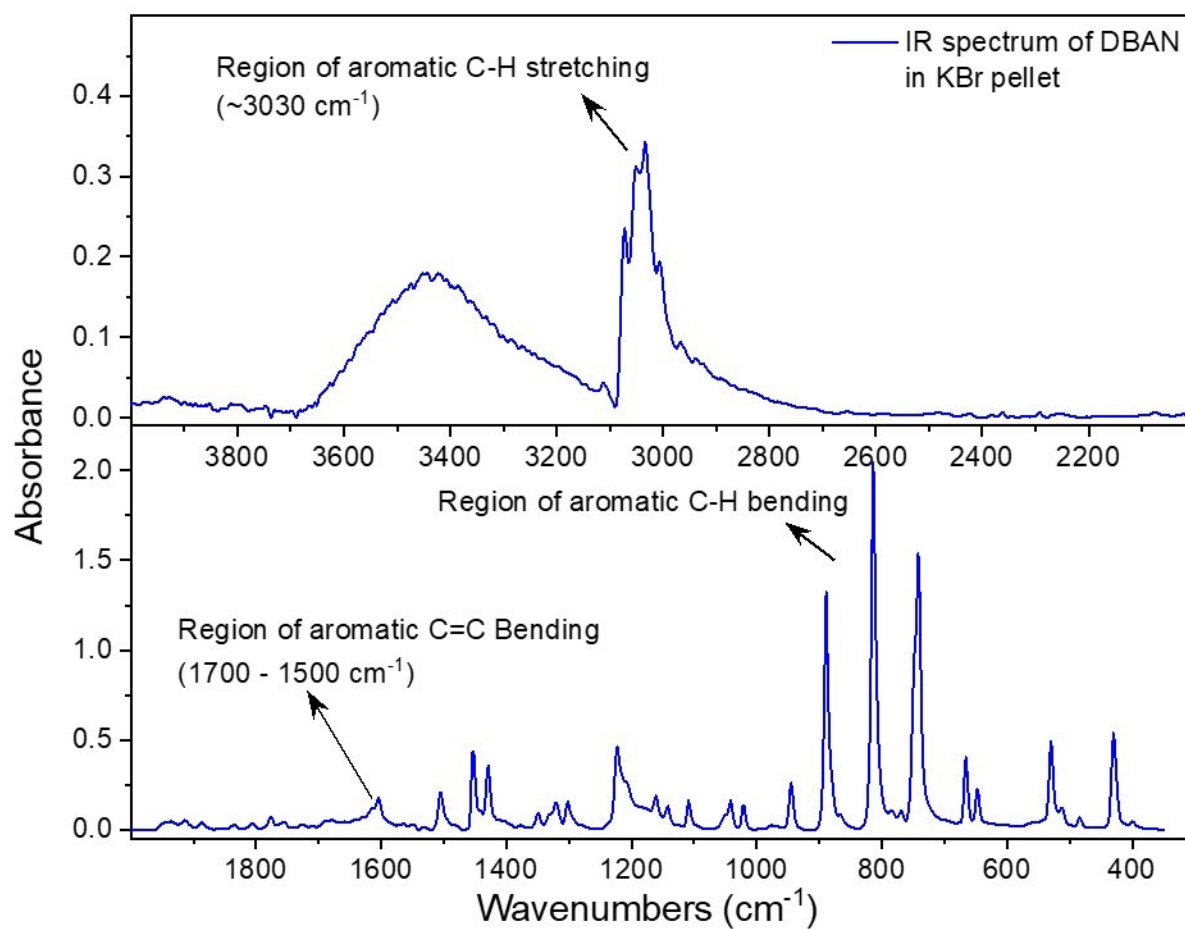


Figure S2. FT-IR spectrum of DBAN in KBr pellet recorded under ambient atmosphere.

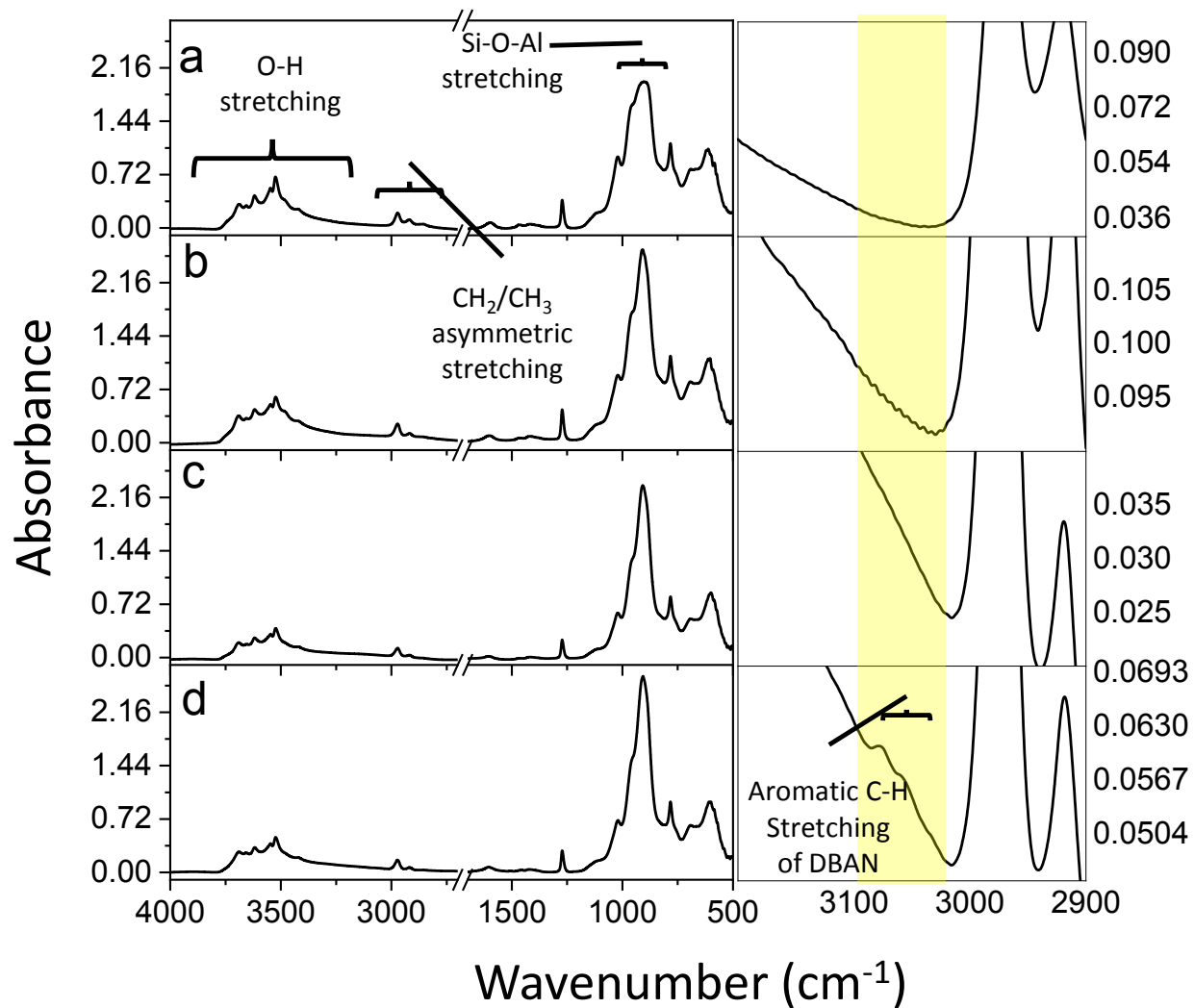


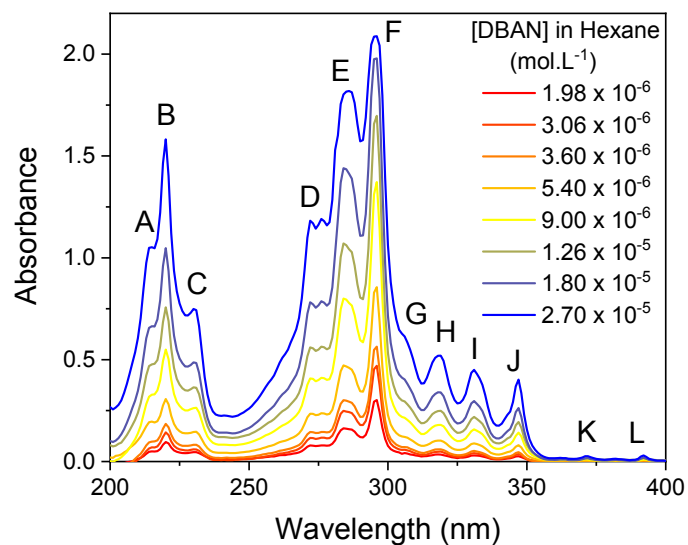
Figure S3. FT-IR spectra of thin films, prepared from pristine Imo-CH₃ (a) and Imo-CH₃ loaded with DBAN at loading concentrations of $9 \times 10^{-6} \text{ mol}\cdot\text{g}^{-1}$ (b), $3.1 \times 10^{-5} \text{ mol}\cdot\text{g}^{-1}$ (c) and $8.1 \times 10^{-4} \text{ mol}\cdot\text{g}^{-1}$ (d).

Table S2. Assignment of the vibrational bands of Imo-CH₃ and DBAN^{3,5,6}

Sample	Wavenumber of absorption bands (cm ⁻¹)	Assignment
	419	O-Al-O bending
	508	O-Si-O bending
	570/548	Al-O modes
	684	Al-O modes
	780	CH ₃ rocking and Si-C stretching
	956/900	Si-O-Al stretching
	1270	symmetric deformation of CH ₃ in Si-CH ₃
	2980-2910	CH ₂ /CH ₃ asymmetric stretching
	4000-3000	O-H stretching
DBAN	700-900	aromatic C-H bending
	1700-1500	aromatic C=C bending
	~3030	aromatic C-H stretching

4. UV-Vis absorption spectra of DBAN in hexane

(a)



(b)

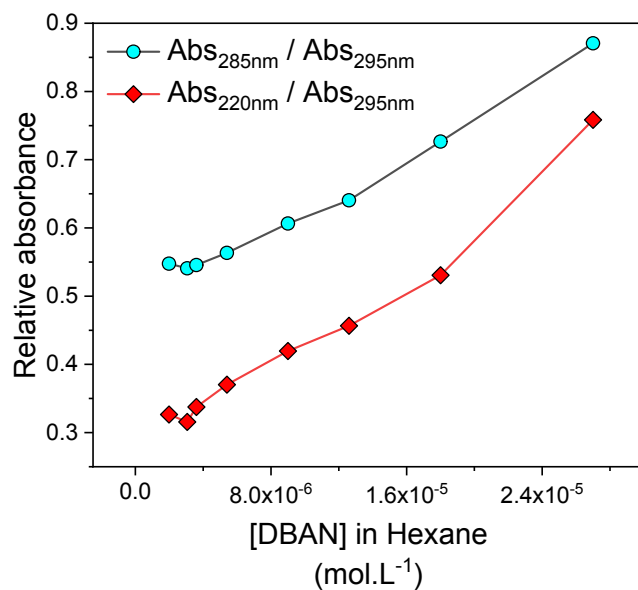


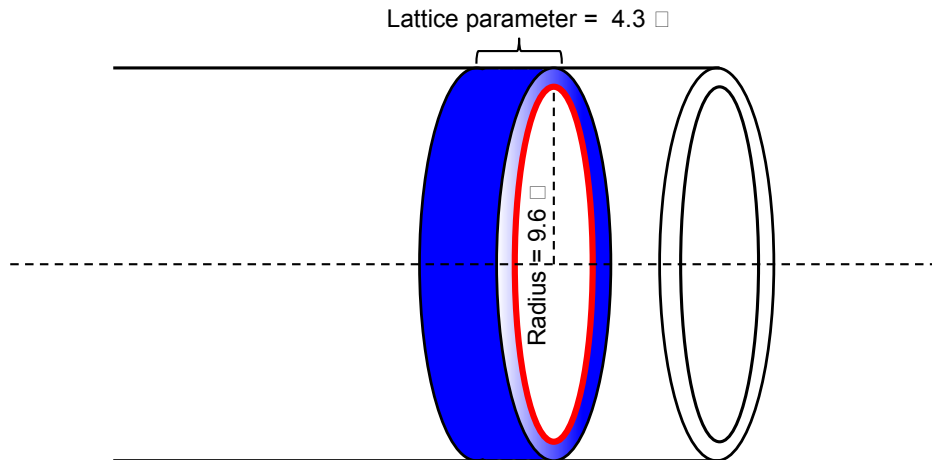
Figure S4. UV-Vis absorption spectra of DBAN in hexane at varying concentrations (a) and concentration dependence of the relative absorbances between 285 and 295 nm (E, F) and between 220 and 295 nm (B, F) (b).

5. Determination of loading concentration of DBAN in Imo-CH₃ nanotubes

The molar mass of a unit lattice ring of Imo-CH₃ is 196 g·mol⁻¹. The volume (v_1) of a unit lattice ring of Imo-CH₃ (shown in Scheme S1; blue ring) can be calculated using the lattice parameter (4.3 Å) and the internal radius (9.6 Å) and was found to be 1244.3 Å³. For a DBAN-loaded Imo-CH₃ sample, the increase in internal electron density (δ_e) was determined by SAXS (Table 1 of the main text). It was found to be 0.06 e⁻·Å⁻³. The average number of DBAN molecules present per unit lattice ring of Imo-CH₃ was calculated using the lattice ring volume (v_1), the increase in electronic density (δ_e) and the number of electrons in a DBAN molecule (146 electrons per DBAN). It is 0.51 DBAN per unit lattice ring (roughly one DBAN molecule per two unit lattice rings). Using the concentration of Imo-CH₃ in aqueous solution (7.5 g·L⁻¹), the concentration of DBAN in aqueous Imo-CH₃ solution could then be obtained in mol·L⁻¹. Finally, the molar extinction coefficient (ϵ , L·mol⁻¹·cm⁻¹) of DBAN in Imo-CH₃ aqueous solution at a given wavelength was obtained using Beer-Lambert's law:

$$\epsilon = \frac{A_\lambda}{c \times l} \quad (\text{Eq. S1})$$

where A_λ is the absorbance of the DBAN-loaded Imo-CH₃ solution (for which the δ_e was measured by SAXS) at a given wavelength λ (nm); c is the concentration of DBAN in mol·L⁻¹; and l is the cell pathlength in cm.



Scheme S1. Schematic representation of the unit lattice ring in Imo-CH₃ nanotube.

6. Relative intensity between two peaks in UV-Vis spectrum of DBAN in hexane (a) and of DBAN encapsulated in Imo-CH₃ aqueous solutions (b-d).

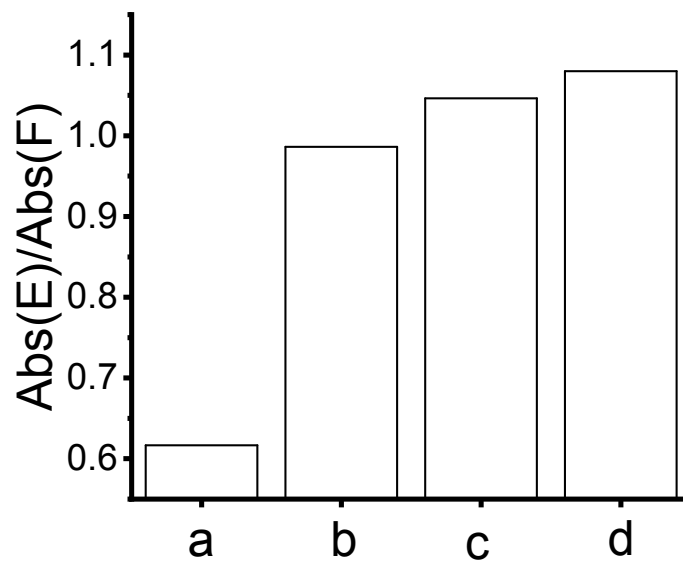


Figure S5. Relative intensity between (E, F) obtained from Figure 3(a-d).

7. Wavelength maxima in UV-Vis absorption spectra of DBAN.

Table S3. Wavelength maxima measured in the UV-Vis absorption spectra of DBAN in hexane and in Imo-CH₃ solutions.

Maximum	Position of wavelength maximum (nm)			
	Conc. of DBAN in Hexane (mol·L ⁻¹)	Conc. of DBAN encapsulated in Imo-CH ₃ (mol·g ⁻¹)		
	1.1×10^{-5}	9×10^{-6}	3.1×10^{-5}	8.1×10^{-4}
A	214	214	214	--
B	220	220	220	223
C	231	231	--	--
D	272	272	--	--
E	285	286	287	292
F	295	297	298	300
G	306	--	--	--
H	318	320	322	--
I	331	333	335	340
J	347	349	351	357
K	371	--	--	--
L	393	393	393	400

8. Relative intensity between peaks measured in the fluorescence emission spectrum of DBAN in hexane (a) and of DBAN encapsulated in Imo-CH₃ in aqueous solution (b-d).

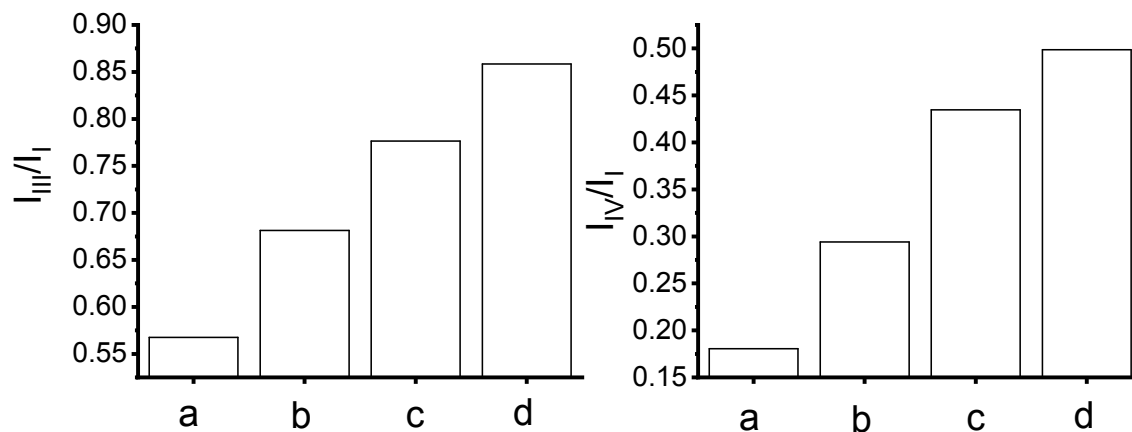


Figure S6. Relative intensity between different peaks measured in fluorescence emission spectra (Figure 4 in the main text).

9. Wavelength maxima in fluorescence emission spectra of DBAN.

Table S4. Different wavelength maxima in the fluorescence emission spectra of DBAN in hexane and in Imo-CH₃ solutions.

Emission Maximum	Position of wavelength maximum (nm)			
	Conc. of DBAN in Hexane (mol·L ⁻¹)	Conc. of DBAN encapsulated in Imo-CH ₃ (mol·g ⁻¹)		
	1.1×10^{-5}	9×10^{-6}	3.1×10^{-5}	8.1×10^{-4}
I _I	391	392	393	402
I _{II}	402	402	402	--
I _{III}	413	415	416	426
I _{IV}	440	440	442	450
I _V	470	470	--	--

10. Evolution of UV-Vis absorption spectra of DBAN upon UV illumination in hexane under air atmosphere and pre-bubbled with dioxygen and argon

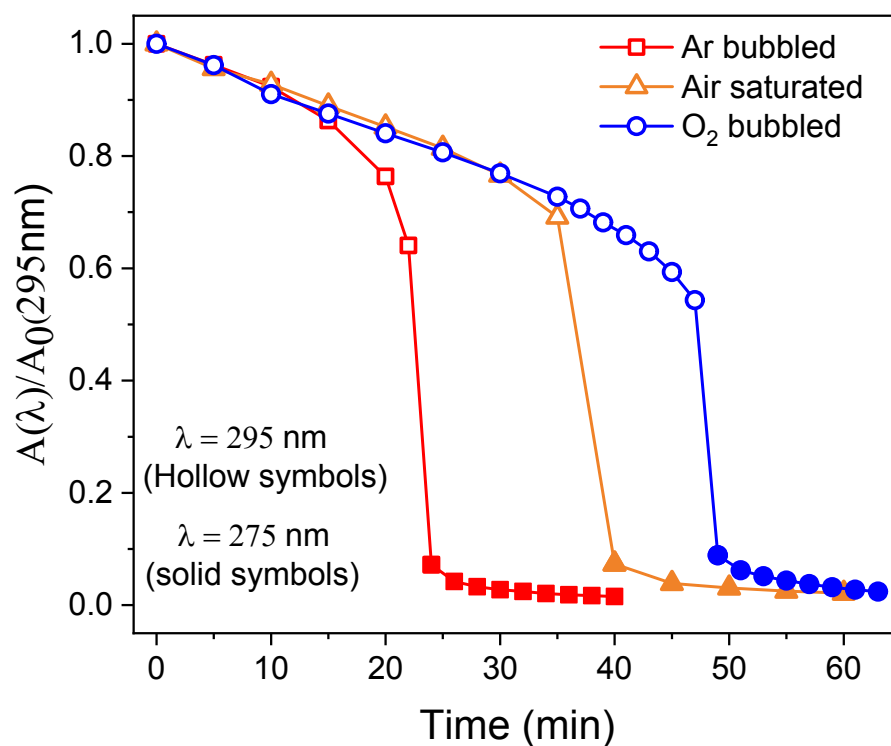


Figure S7. Evolution of the ratio of the absorbance at the maximum wavelength (λ_{max}) and the initial absorbance at 295 nm of DBAN in hexane upon UV illumination under various atmospheres.

11. Relative absorbance between two different wavelengths during UV illumination of air-saturated solutions of DBAN in hexane (derived from Figure 6a in the main text)

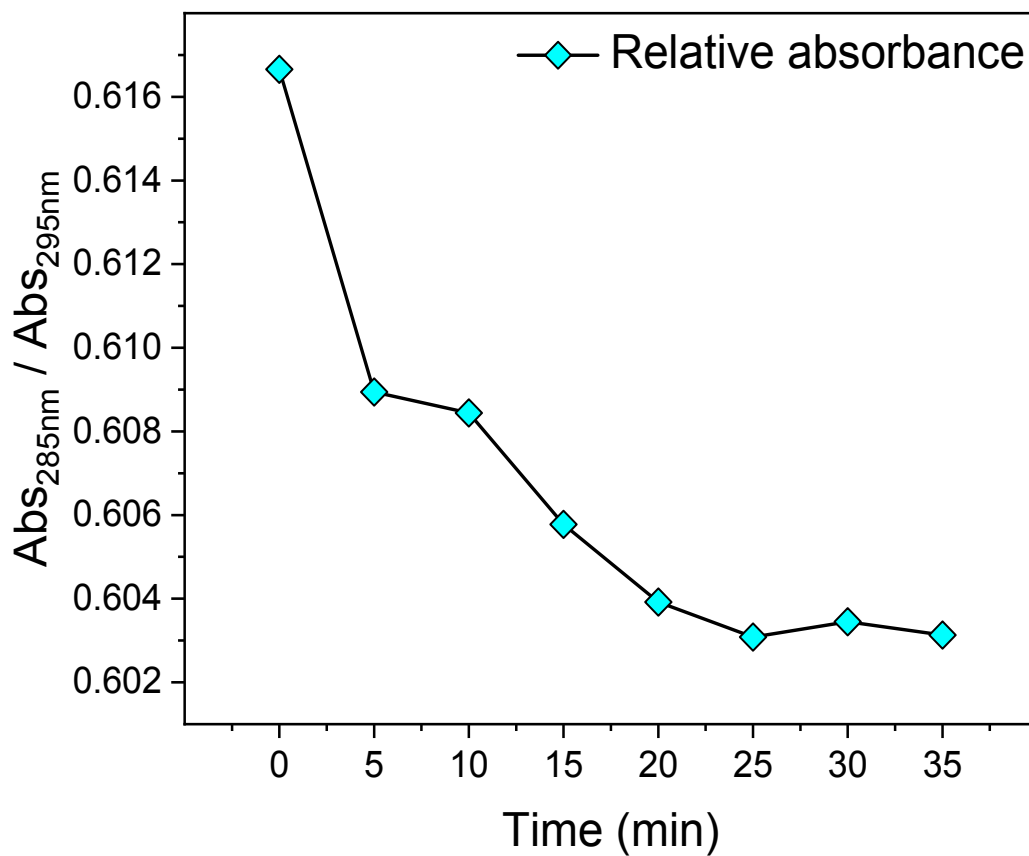


Figure S8. Ratio of absorbance between 285 nm and 295 nm during UV illumination of air-saturated solutions of DBAN in hexane (derived from Figure 6a in the main text).

12. Evolution of UV-Vis absorbance at different wavelengths for encapsulated DBAN at varying loading concentrations

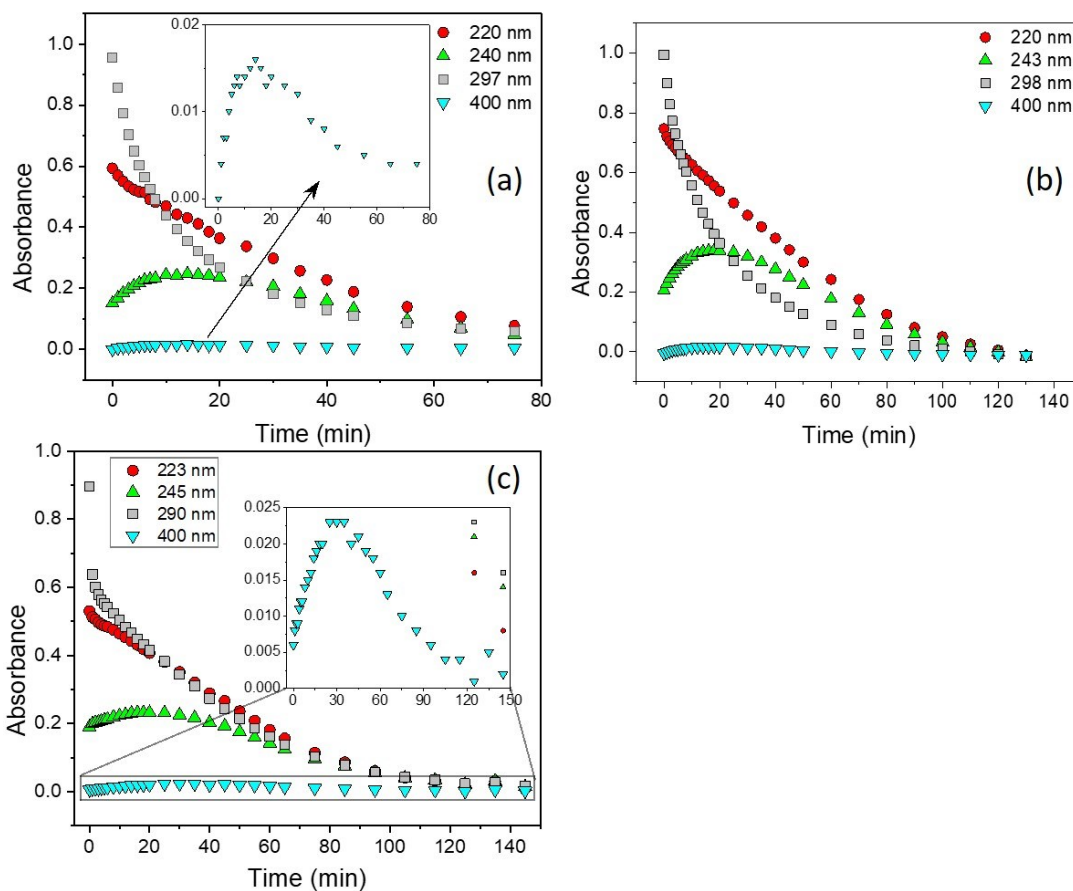


Figure S9. Temporal evolution of UV-Vis absorbance of DBAN, encapsulated in Imo-CH₃ nanotubes in aqueous medium under UV illumination (253.7 nm), with an initial loading concentration of $9 \times 10^{-6} \text{ mol}\cdot\text{g}^{-1}$ (a), $3.1 \times 10^{-5} \text{ mol}\cdot\text{g}^{-1}$ (b) and $8.1 \times 10^{-4} \text{ mol}\cdot\text{g}^{-1}$ (c) at different wavelengths.

13. Time variation of inverse of DBAN concentration in Imo-CH₃ solution under UV illumination and the rate constants.

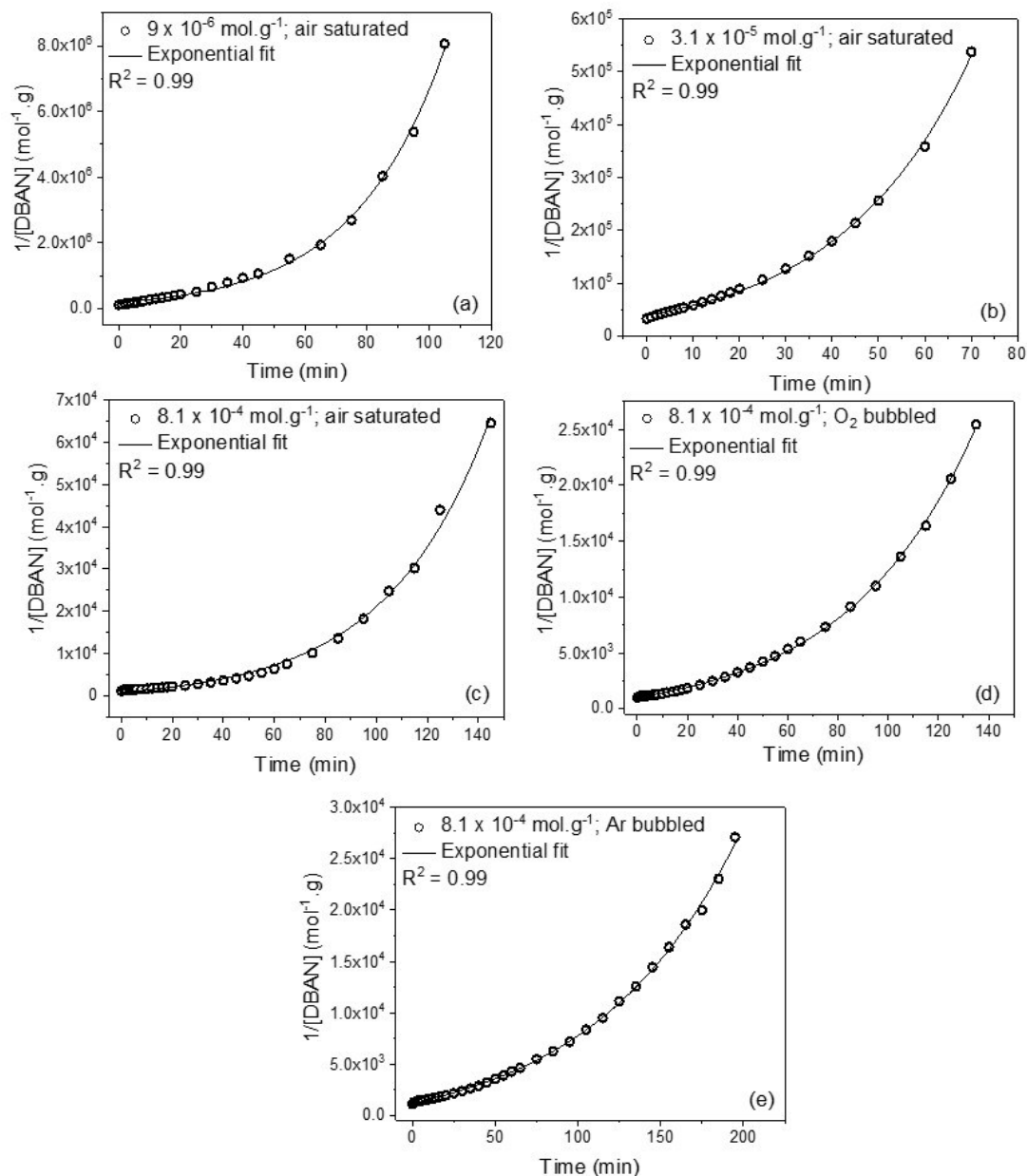


Figure S10. Time variation of inverse of DBAN concentration in Imo-CH₃ nanotubes in aqueous medium and corresponding exponential fit at different loading concentrations and gaseous atmospheres.

Table S5. Rate constants for photo-oxidation (k_1), photo-cycloaddition (k_2) and photo-oxidation quantum yield at 253.7 nm.

DBAN loading concentration (mol·g ⁻¹)	Gaseous atmosphere	Photo-oxidation rate constant k_1 (min ⁻¹)	Photo-cycloaddition rate constant k_2 (min ⁻¹ ·mol ⁻¹ ·g)	Photo-oxidation Quantum Yield at 253.7 nm ϕ_1 (mol·Einstein ⁻¹)
9×10^{-6}	air	3.4×10^{-2}	593	3.33×10^{-3}
3.1×10^{-5}	air	3.5×10^{-2}	114	3.43×10^{-3}
8.1×10^{-4}	air	2.5×10^{-2}	11	2.45×10^{-3}
	O ₂	1.9×10^{-2}	11	1.86×10^{-3}
	Ar	1.1×10^{-2}	11	1.08×10^{-3}

14. Comparison of UV-Vis absorption spectra of DBAN in water and of encapsulated DBAN in Imo-CH₃ aqueous solution

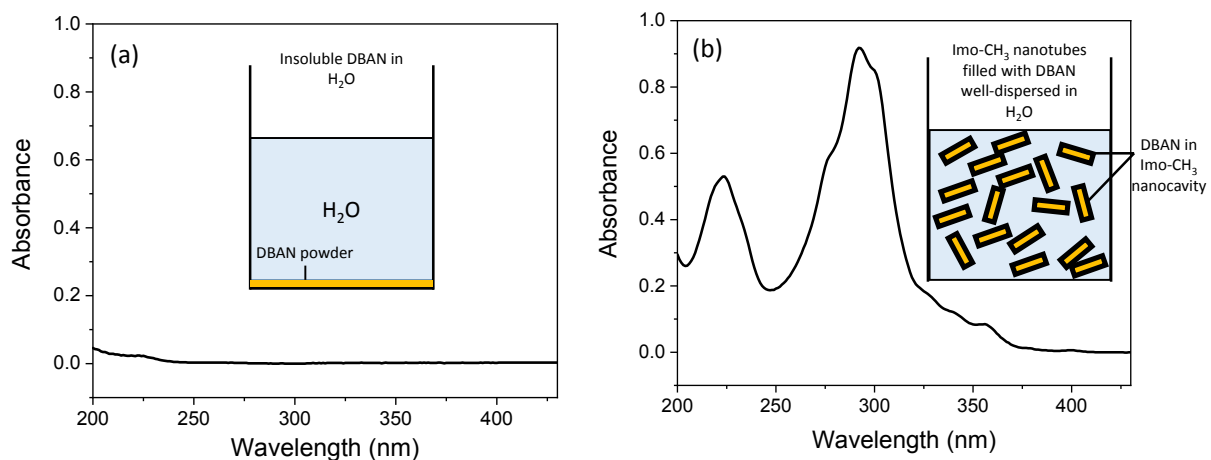


Figure S11. UV-Vis spectrum of water saturated with DBAN (a) and of DBAN-loaded aqueous Imo-CH₃ solution (loading concentration: $8.1 \times 10^{-4} \text{ mol}\cdot\text{g}^{-1}$) (b). Insoluble DBAN powder residue was separated by centrifugation prior to UV-Vis spectroscopy measurement. Solution 'b' was diluted 50 times prior to UV-Vis spectroscopy. In the schemes, the dimensions of the different objects are arbitrarily scaled for visualization purpose only.

15. Stability of Imo-CH₃ nanoreactor under UV illumination

The stability of Imo-CH₃ nanotubes before and after UV illumination was characterized by UV-Vis spectroscopy and FT-IR spectroscopy. 3 mL of the Imo-CH₃ aqueous solution (7.5 mg.mL⁻¹) was placed in a quartz cuvette (1 cm optical pathlength) and illuminated for different times (up to 5 hours) under UV light (253.7 nm, 4.15×10¹⁹ photons.L⁻¹.s⁻¹). Figure S12 shows the UV-Vis spectra of the Imo-CH₃ aqueous solution at regular time intervals during UV illumination. The negligible change observed in the UV-Vis spectra during an illumination of 5 hours suggests that Imo-CH₃ nanotubes are highly stable under high-energy UV radiation.

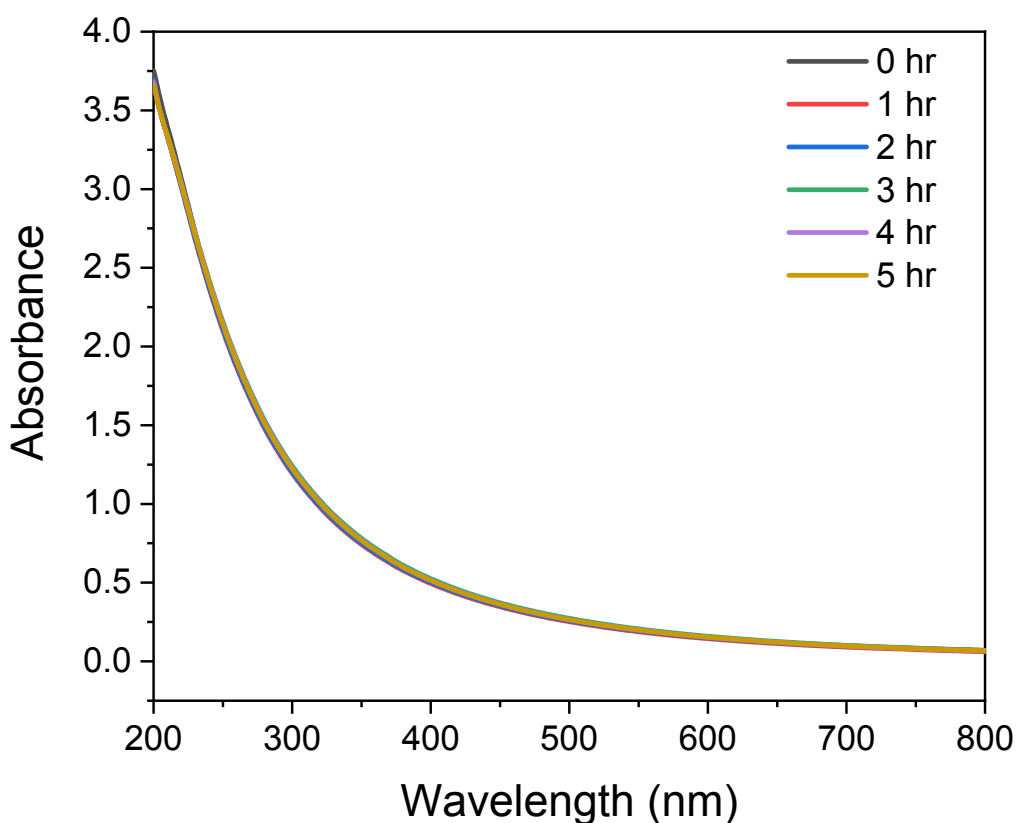


Figure S12. UV-Vis absorption spectra of Imo-CH₃ aqueous solution (7.5 mg.mL⁻¹) under illumination with UV light (253.7 nm, 4.15×10¹⁹ photons.L⁻¹.s⁻¹) for various exposure times. MilliQ water was used as the reference during the measurements.

Figure S13 shows the FT-IR spectra of Imo-CH₃ nanotubes before (a) and after UV illumination for 1 hour (b), 3 hours (c) and 5 hours (d). The change in the FT-IR spectra of pristine and UV-illuminated Imo-CH₃ is negligible. The doublet at 956/900 cm⁻¹, due to Si-O-Al stretching

and characteristic of the tubular structure of Imo-CH₃, as well as the peak at 2980 cm⁻¹, characteristic of -CH₃ asymmetric stretching, do not change upon illumination. This confirms the good stability of Imo-CH₃ nanotubes under high-energy UV radiation during 5 hours of illumination.

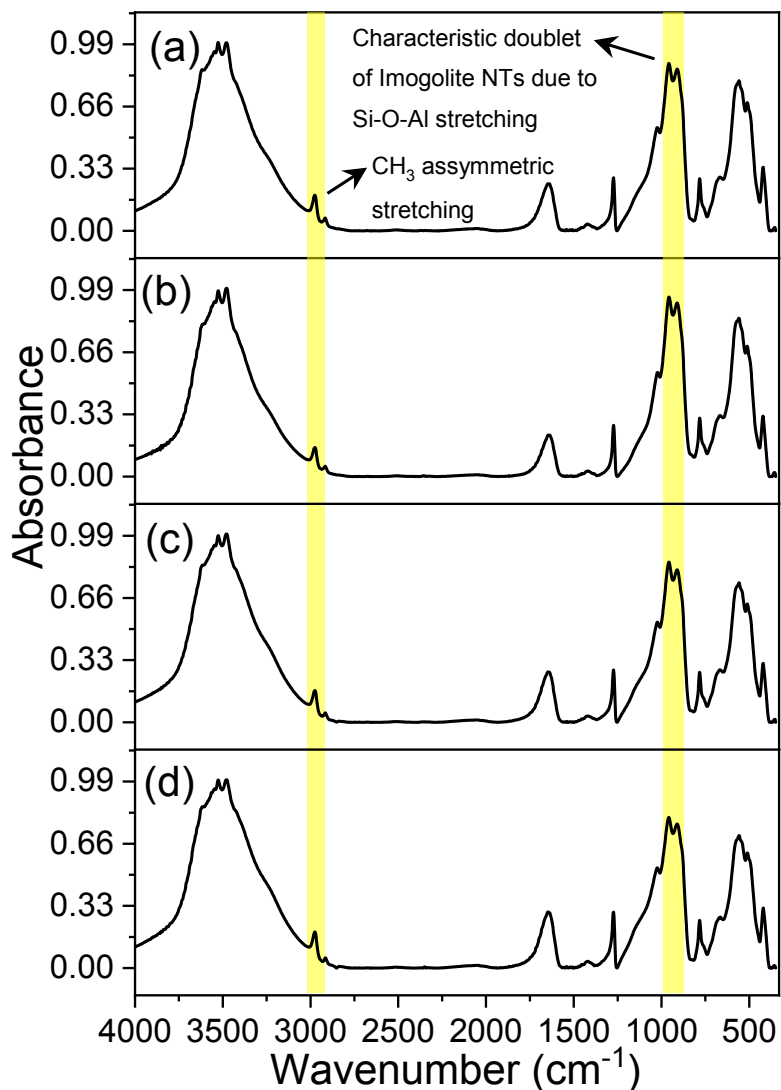


Figure S13. FT-IR spectrum of Imo-CH₃ nanotubes before (a) and after illumination with 253.7 nm UV light in aqueous solution for 1 hour (b), 3 hours (c) and 5 hours (d). Two characteristic infrared bands of Imo-CH₃ nanotubes (vibrational signature of methyl groups and of the nanotubes) are shown with a yellow color.

16. Possible mechanism of DBAN mineralization.

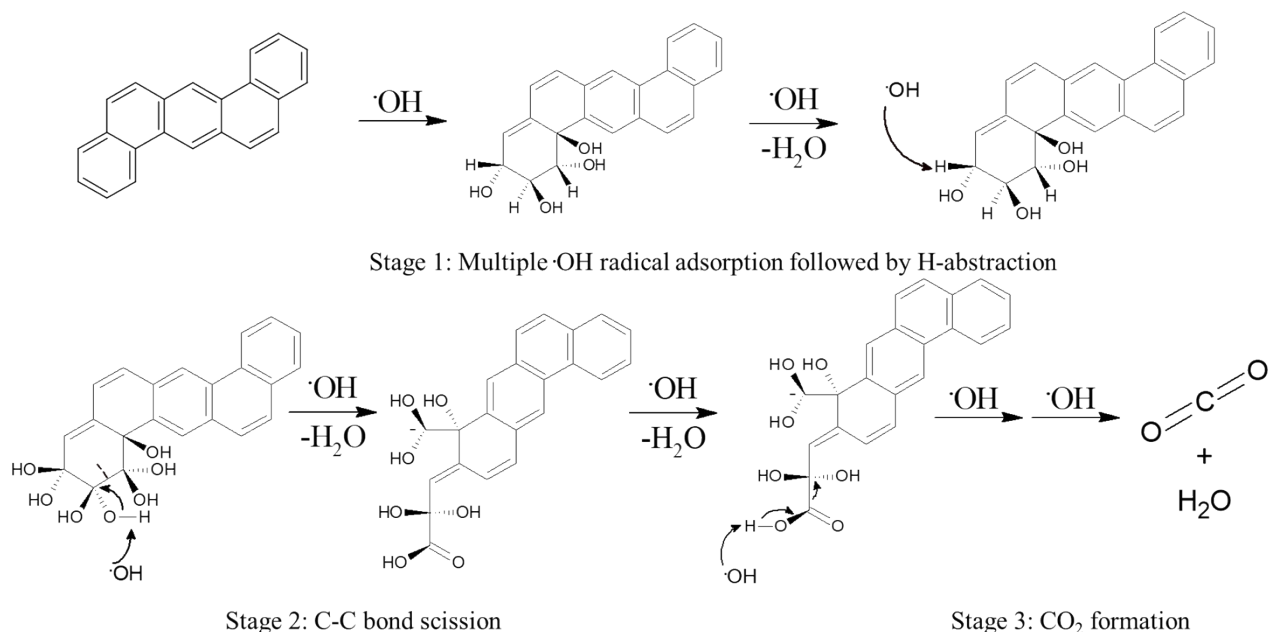


Figure S14. Possible mechanism of DBAN mineralization by $\cdot\text{OH}$ radicals.

References

1. A. Thill, P. Picot, L. Belloni, A mechanism for the sphere/tube shape transition of nanoparticles with an imogolite local structure (imogolite and allophane), *Applied Clay Science* 2017, **141**, 308-315.
2. P. Du, P. Yuan, A. Thill, F. Annabi-Bergaya, D. Liu, S. Wang, Insights into the formation mechanism of imogolite from a full-range observation of its sol-gel growth, *Applied Clay Science* 2017, **150**, 115-124.
3. Y. Liao, P. Picot, J-B. Brubach, P. Roy, S. Le Caër, A. Thill, Self-supporting thin films of imogolite and imogolite-like nanotubes for infrared spectroscopy, *Applied Clay Science* 2018, **164**, 58.
4. D.V. Kazachkin, Y. Nishimura, H.A. Witek, Stephan Irle, E. Borguet, Dramatic reduction of IR vibrational cross sections of molecules encapsulated in carbon nanotubes, *J. Am. Chem. Soc.* 2011, **133**, 8191–8198.
5. Y. Liao, P. Picot, M. Lainé, J-B. Brubach, P. Roy, A. Thill, S. Le Caër, Tuning the properties of confined water in standard and hybrid nanotubes: An infrared spectroscopic study, *Nano Research* 2018, **11(9)**, 4759.
6. S. Singh, C. Sandorf, Infrared spectra of photodimers of anthracene, benzo[a]anthracene, and tetracene, *Canadian J. Chem.* 1969, **47**, 257.